On the Creep Analysis of Rock Masses by Using a Viscoelastoplastic Model

A. A. Jameei(✉), A. Azami, S. Moallemi, K. Dang, and T. Yacoub

Rocscience Inc, Toronto, ON, Canada
amir.jameei@rocscience.com

Abstract. Creep in rock masses is typically described as the gradual deformation that occurs when loads are applied for long durations at varying temperatures. This process, which may result from chemical reactions in susceptible environments, leads to instabilities and catastrophic strength degradation in the rock masses. An example of a susceptible environment is crystalline and sedimentary host rocks or rock salts in deep geological repositories. Such environments are subject to the long-term transfer of radionuclides at high temperatures. This research is focused on the study of creep in several numerical examples under different loading conditions. The simulations are conducted using finite element analysis of viscoelastic and viscoelastoplastic materials. The former uses the known Waste Isolation Pilot Plant (WIPP) model, and the latter incorporates a newly proposed viscoelastoplastic model that integrates the WIPP and Mohr-Coulomb (MC) models. Results are verified with available closed-form and numerical solutions.

Keywords: Time-dependent Deformation · Waste Isolation Pilot Plant · Rock Masses · Finite Element · Viscoelastoplasticity

1 Introduction

The standard plasticity procedure, known as classical elastoplasticity, utilizes the additivity postulate of infinitesimal strain rates. It involves using a yield criterion, a flow rule, Hook's law, and Prager's consistency condition. The yield criterion limits the elastic response, the flow rule describes plastic deformation, Hook's law explains elastic deformation, and Prager's consistency condition ensures that the system of equations is consistent, i.e., the number of equations equals the number of unknowns. An extensive study regarding the classical plasticity framework can be found in the books of Khan and Huang [5] and Pietruszczak [8].

Elastoplastic behavior refers to a deformation process that is not affected by the rate at which it occurs. On the other hand, viscous materials exhibit rate-dependent deformation, where the rate of application of loads influences energy dissipation during loading and unloading. Models based on various combinations of spring-dashpot-slider idealizations are commonly used to study such problems. These models decompose the strain rate into two parts: elastic and viscoplastic. The elastic part follows Hook's law, while the viscoplastic part is described by models such as Perzyna and Duvaut-Lions that

R. E. Hammah et al. (Eds.): RIC 2023, AHE 19, pp. 264–277, 2023.
https://doi.org/10.2991/978-94-6463-258-3_28

allow for positive yield functions or formulations incorporating evolving yield surfaces based on internal variables (Simo & Hughes, 1988). These internal variables depend on strain rates and measures of accumulated plastic strain or work. Deformations are purely elastic if the stress state does not reach the elastic limit (initial yield surface). This study introduces a simple procedure that separates the dependence of viscous and plastic deformation. In other words, materials can exhibit time-dependent deformations under the proposed procedure even if the yield function is less than zero. The proposed procedure involves an idealization of springs, dashpots, and sliding parts arranged in series.

The WIPP-reference models are commonly used for studying rocks' time-dependent deformation near radioactive waste repositories. Initially, these models were introduced to describe viscoelastic behavior [1–4, 11, 12]. Later, the WIPP-reference model by Itasca Consulting Group Inc. [3–4] was extended to incorporate a Drucker-Prager yield function to account for irreversible deformations. The current study expands the WIPP-reference creep formulation to include the Mohr-Coulomb yield function. This study's proposed model, WIPP-MC, incorporates the simple viscoelastoplastic procedure explained in the previous paragraph. The applicability of the current model in finite element analysis is demonstrated through various numerical examples.

2 Constitutive Relations

Conventions: The indicial (Einstein) notation is used throughout this section (a reference for index notation). In addition, the Cartesian coordinate system is used in the formulations. Also, the normal stresses are assumed to be positive in tension.

Detailed derivations of the original WIPP model for viscoelastic materials can be found in van Sambeek [12] and Itasca Consulting Group Inc. [3–4] (Program Guide: Constitutive Models). However, this study briefly addresses the original model for completeness.

The original WIPP-reference model does not account for the volumetric time-dependent deformations. Accordingly, the additivity postulate of the rate of infinitesimal strains results in

$$\dot{\varepsilon}_{ij} = \dot{\varepsilon}_{ij}^{vs} + \dot{\varepsilon}_{ij}^{e} + \dot{\varepsilon}_{ij}^{p} \tag{1}$$

where $\dot{\varepsilon}$ denotes the material time derivative, $\dot{\varepsilon}_{ij}$ is the rate of strain tensor, and the superscripts e, p, and vs refer to elastic, plastic, and viscous shear parts, respectively.

The viscous shear strain rate is assumed to be coaxial with the direction of the deviatoric stress tensor [12]. Accordingly, $\dot{\varepsilon}_{ij}^{vs}$ is given as,

$$\dot{\varepsilon}_{ij}^{vs} = \frac{\sqrt{3}\dot{\epsilon}}{2\sqrt{J_2}} s_{ij} \tag{2}$$

where J_2 denotes the second invariant of the deviatoric stress tensor ($J_2 = \frac{1}{2} s_{ij} s_{ij}$; where $s_{ij} = \sigma_{ij} - \sigma_{kk}\delta_{ij}/3$) and $\dot{\epsilon}$ is a temperature-dependent parameter that consists of primary ($\dot{\epsilon}_p$) and secondary parts ($\dot{\epsilon}_s$) according to

$$\dot{\epsilon} = \dot{\epsilon}_p + \dot{\epsilon}_s \tag{3}$$

where

$$\dot{\epsilon}_s = D\left(\frac{\sqrt{3J_2}}{F_d}\right)^n \exp\left(-\frac{Q}{RT}\right) \tag{4}$$

$$\dot{\epsilon}_p = \begin{cases} \left(A - B\epsilon_p\right)\dot{\epsilon}_s\dot{\epsilon}_s \geq \dot{\epsilon}^*_{ss} \\ \left(A - B\left(\frac{\dot{\epsilon}^*_{ss}}{\dot{\epsilon}_s}\right)\epsilon_p\right)\dot{\epsilon}_s\dot{\epsilon}_s < \dot{\epsilon}^*_{ss} \end{cases} \tag{5}$$

where Q is the activation energy, T denotes the temperature in Kelvin, R is the universal gas constant, and A, B, D, n, and $\dot{\epsilon}^*_{ss}$ are material constants of the original WIPP model. It should be noted that ϵ_p is an internal parameter and accumulates over time.

According to the flow rule,

$$\dot{\varepsilon}^p_{ij} = \dot{\lambda}\frac{\partial g}{\partial \sigma_{ij}} \tag{6}$$

where g is a potential function and $\dot{\lambda}$ is a plastic multiplier. It should be noted that if g is equal to the yield function f, the rule is called associated - and if not, it is called nonassociated. The Mohr-Coulomb f is used, and g is chosen to be similar to (but not equal to) the form of f [7]. Accordingly,

$$\begin{cases} f = \sqrt{3J_2} + MI_1/3 - Nc = 0 \\ g = \sqrt{3J_2} + M_\psi I_1/3 = const. \end{cases} \tag{7}$$

where $I_1 = \sigma_{kk}$. In addition, c is a material constant (cohesion), and

$$\begin{cases} N = \frac{3\cos\phi}{\sqrt{3}\cos\theta - \sin\theta\sin\phi} \\ M = \frac{3\sin\phi}{\sqrt{3}\cos\theta - \sin\theta\sin\phi} \\ M_\psi = \frac{3\sin\psi}{\sqrt{3}\cos\theta - \sin\theta\sin\psi} \end{cases} \tag{8}$$

In Eq. (8), ϕ and ψ are friction and dilation angles, and

$$\sin 3\theta = -\frac{3\sqrt{3}}{2}\frac{J_3}{J_2^{3/2}} \tag{9}$$

where θ denotes the Lode angle and J_3 is the third invariant of the deviatoric stress tensor ($J_3 = s_{ij}s_{jk}s_{ki}$). It should be noted θ follows the representation provided by Nayak and Zienkiewicz [6].

It should be noted that the cutting plane approach is used for the numerical integration (stress update) of the current constitutive relations. The cutting plane approach is a two-step algorithm that evaluates an elastic (here: viscoelastic) predictor and a plastic corrector [10]. Details of the stress update of the current model were not explained in this article for brevity. The WIPP-MC model presented in this study is implemented in the finite element software RS2 [9] as a new user-defined.dll file.

3 Numerical Examples

In order to verify the applicability of the current model in finite element analyses, seven different examples are presented in this section.

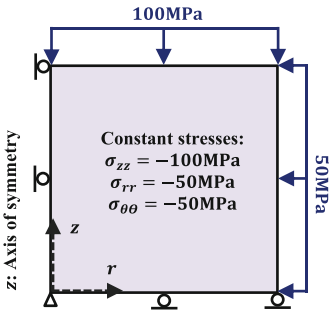

Fig. 1. Boundary and initial conditions of the constant stress triaxial test

Table 1. Material parameters of the constant stress triaxial test

Parameter	Value	Unit
Gas constant, R	1.987	cal/(molK)
Activation energy, Q	12000	cal/mol
WIPP model exponent, n	4.9	
WIPP model constant, A	4.56	
WIPP model constant, B	127	
WIPP model constant, D	1.4544×10^{-6}	$\text{MPa}^{-\text{n}}\text{s}^{-1}$
Critical steady-state creep rate, $\dot{\epsilon}^*_{ss}$	5.39×10^{-8}	s^{-1}
Temperature, T	300	K

3.1 Constant Stress Triaxial Test (Creep Test)

This example deals with an axisymmetric finite element analysis of a cylindrical rock mass with a radius and a height of 1m under constant stresses (Fig. 1). The constant stresses are applied to the domain by assuming fixed radial and axial stresses throughout the domain in equilibrium with the corresponding boundary tractions (Fig. 1). The spatial discretization contains only a single eight-nodded quadrilateral element. The radial and axial stresses are −50 MPa and −100MPa, respectively. The model constants are given in Table 1.

As depicted in Fig. 2, the material deforms over time under constant stress and temperature, and the finite element results coincide precisely with the closed-form solutions.

3.2 Restrained Triaxial Test (Relaxation Test)

The domain of the analysis and spatial discretization of this example are similar to those of the first example, but the boundaries are assumed to be stationary. The stationary boundaries result in achieving no deformation since the material is homogenous. The

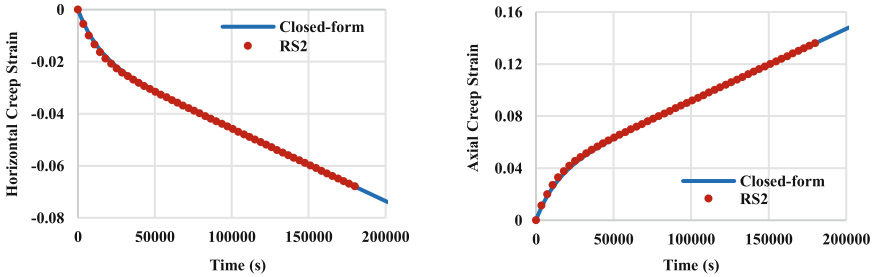

Fig. 2. Finite element (RS2) result compared with the closed-form solution

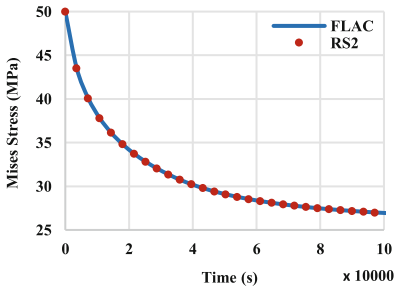

Fig. 3. Finite element (RS2) result compared with finite difference (FLAC) result for the restrained triaxial test

material constants are kept similar to those of the first example; also: $K = 971.4$MPa and $G = 300$MPa. An initial triaxial state of stress is applied to the domain. The radial and axial stresses are -50 MPa and -100 MPa, respectively. Figure 3 shows the result of this example.

As expected, the Mises stress reduces as time goes on (Fig. 3). The RS2 finite element results match precisely with the finite difference results of FLAC.

3.3 Simple Shear Test

The simple shear test is conducted on a domain of 1m $\times$ 1m under the plane strain condition. The finite element mesh comprises four 3-nodded triangular elements (Fig. 4). The material constants are similar to those of the restrained triaxial test. However, the analysis is conducted at different velocities. In other words, a constant horizontal displacement of 0.01m is applied to the top edge of the domain at different times. The results of the analysis are depicted in Fig. 5.

As shown in Fig. 5, the developed shear stress decreases as time increases. In other words, as the displacement is applied over lower velocities, the results approach the closed-form solution when there is no creep. The current results match precisely those obtained in FLAC.

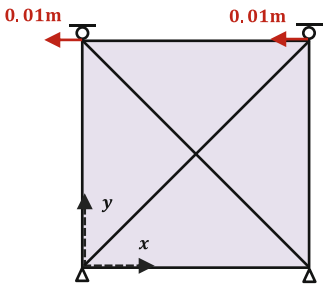

Fig. 4. Boundary conditions of the simple shear test

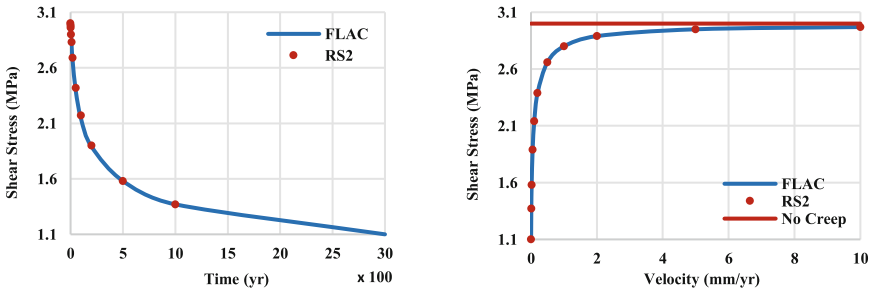

Fig. 5. Finite element (RS2) result compared with finite difference (FLAC) result for the simple shear test

3.4 Parallel-Plate Viscometer

This example is kept from Itasca's Verification and Example Problems, subsection WIPP-Type Models: Parallel-Plate Viscometer. It is aimed to study the creep behaviour by using finite element analysis. The analysis domain is a viscoelastic material with $K = 20700$ MPa and $G = 12400$ MPa and the dimension of 20 m $\times$ 10 m, which is steadily squeezed between two rigid parallel plates that are moving at a constant velocity of 10^{-9} m/s for a total duration of 2500 h. High cohesion and tensile strength are assigned to the material to guarantee that the stress state lies under the yield surface so that the material exhibits a viscoelastic response. The rest of the material constants are kept similar to those of the constant stress triaxial example.

Under the symmetry advantages, only one-quarter of the domain is analyzed. Some constant virtual forces are applied to the domain's lateral (right-hand side) edge, as introduced in the original reference. Boundary conditions and finite element mesh of the implemented RS2 model are depicted in Fig. 6. The finite element mesh contains four-nodded quadrilateral elements.

Figures 7a and 7b show the horizontal displacement for when there is no creep, and there is a creep, respectively. As can be seen from this figure, the creep behaviour results in pronounced horizontal deformation.

A parametric study of this example is depicted in Fig. 8 at different times. It can be observed that as time goes on, the horizontal displacement increases. The results also match with FLAC.

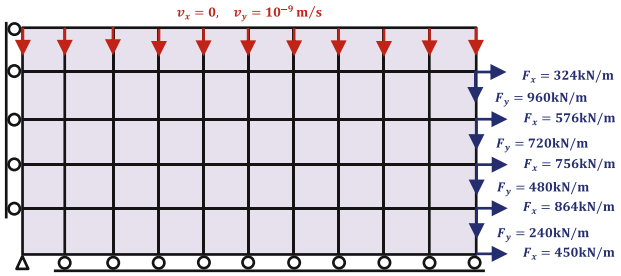

Fig. 6. Boundary conditions of the parallel-plate viscometer

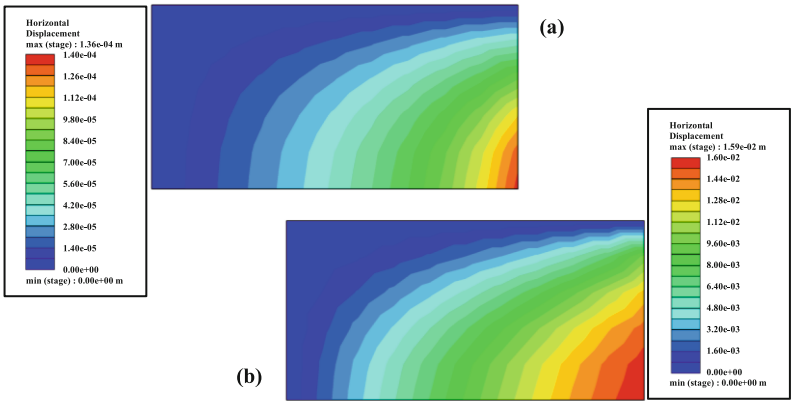

Fig. 7. Distribution of the horizontal displacement (m) at (a) $t = 0$; (b) $t = 2500$hr

3.5 Cylindrical Cavity

This example studies stress distribution in a large domain containing a small cylindrical cavity where the far-field radial stress is kept at −30MPa (Fig. 9). The analyses are conducted under the plane strain condition. In order to verify the applicability of the current creep model in finite element simulations, the domain of the analysis is assumed to be both viscoelastic and viscoelastoplastic. The material constraints are given in Table 2. The finite element mesh contains 840 eight-nodded quadrilateral elements. The finite element mesh and the boundary conditions are depicted in Fig. 9. The outer and inner radii are 21m and 1m, respectively.

Figures 10 and 11 show an agreement between the RS2 results with the closed-form and FLAC solutions.

3.6 Conventional Triaxial Test

In this example, a conventional triaxial test on a cylindrical sample of a viscoelastoplastic rock mass is conducted under an axisymmetric condition. The radius and height of the

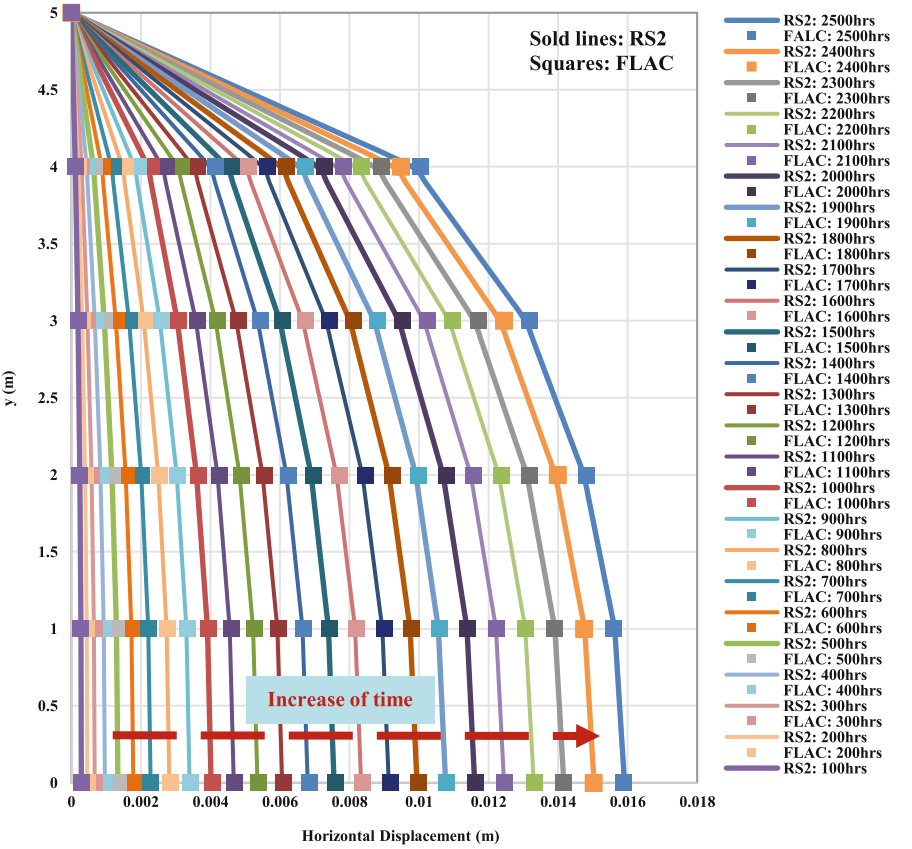

Fig. 8. Finite element (RS2) result compared with finite difference (FLAC) result for the viscometer test at different times

cylinder are both 1m (Fig. 10). The spatial discretization contains only a single eight-nodded quadrilateral element. The initial radial and axial stresses are −10 MPa. The model constants are given in Table 3 (Fig. 12).

Figure 13 depicts that the RS2 result precisely coincides with the FLAC.

3.7 Excavation

In this example, the predictive ability of the current creep model in assessing the settlement induced due to the excavation of a trench and a tunnel is illustrated. The creep constants of this example are identical to those of the conventional triaxial test. However, elastic and shear strength properties of the layers are $K = 833.3$ MPa, $G = 1153.9$ MPa, $c = 3$ MPa, $t = 3$ MPa, $\phi = 40°$, and $\psi = 0°$. The configuration of the problem and the utilized finite element mesh are illustrated in Fig. 14. The finite element mesh consists of 6-nodded (quadratic) triangular elements.

Figure 14 also shows the configuration at different stages of the analysis. The stages include:

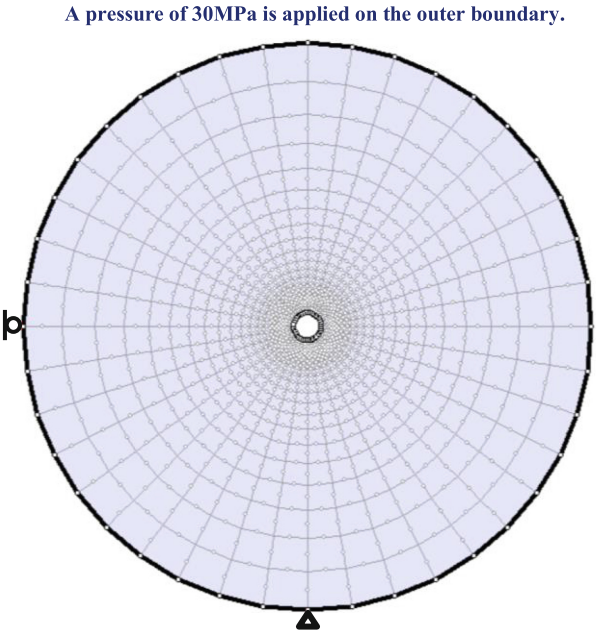

Fig. 9. Boundary condition and finite element mesh of the cylindrical hole example

Table 2. Model constants of the cylindrical hole example

Parameter	**Value**	**Unit**
Cohesion, c	10	MPa
Friction angle, ϕ	0	Degree
Dilation angle, ψ	0	Degree
Shear modulus, G	300	MPa
Bulk modulus, K	971.4	MPa
Gas constant, R	1.987	cal/(molK)
Activation energy, Q	12000	cal/mol
WIPP model exponent, n	3	
WIPP model constant, A	0	
WIPP model constant, B	0	
WIPP model constant, D	1.7535×10^{-6}	$\mathrm{MPa}^{-\mathrm{n}}\mathrm{s}^{-1}$
Temperature, T	300	K

Stage 1: Bringing the domain into equilibrium ($t = 0$)
Stage 2: Excavating the tunnel ($t = 0$)
Stage 3: Excavating the trench ($t = 0$)

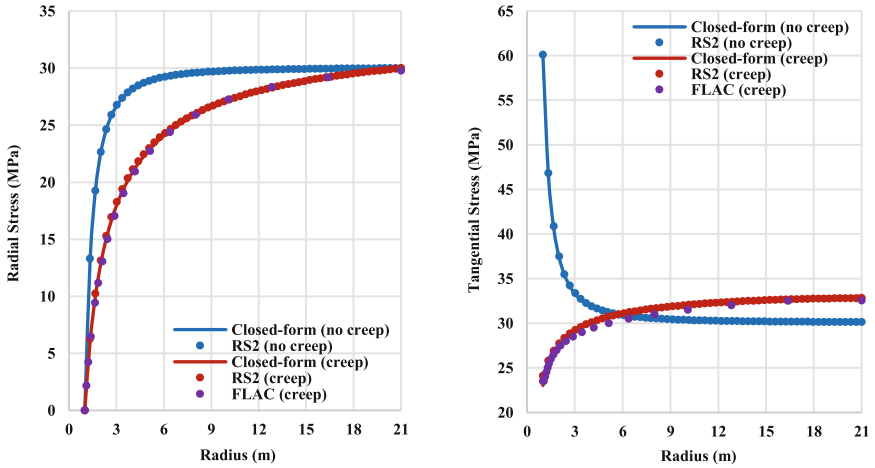

Fig. 10. Finite element (RS2) results compared with closed form solutions and finite difference (FLAC) results for the cylindrical cavity in a viscoelastic domain

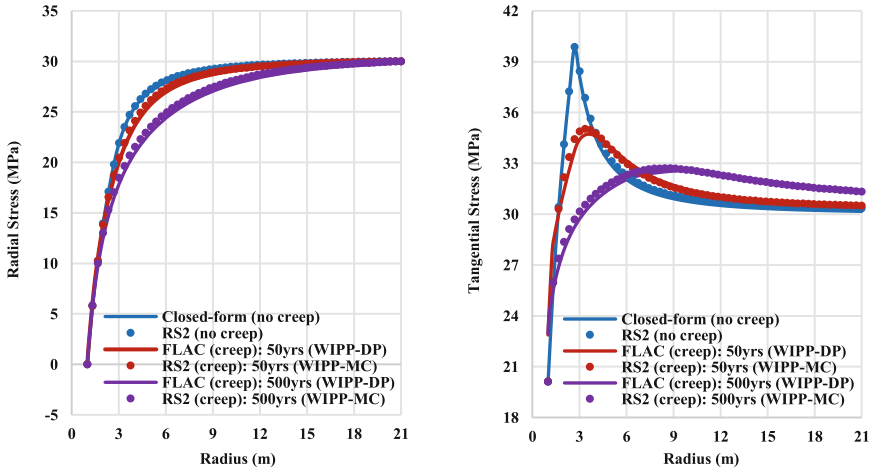

Fig. 11. Finite element (RS2) results compared with the finite difference (FLAC) results for the cylindrical cavity in a viscoelastoplastic domain

Stage 4: Applying the surface foundation load ($t = 0$)
Stages 5–104: Creep analysis under sustained loads ($t = 10$yr)

Figure 15 shows that as time goes on, the deformation exceeds due to creep.

4 Conclusions

A new viscoelastoplastic model is proposed to study the creep behaviour of rocks in the vicinity of radioactive waste repositories. This model is an extension of WIPP-reference to cover irreversible deformations and uses the Mohr-Coulomb yield function.

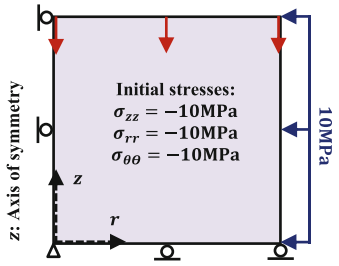

Fig. 12. Boundary and initial conditions of the conventional triaxial test

Table 3. Model constants of the conventional triaxial test

Parameter	**Value**	**Unit**
Cohesion, c	3	MPa
Friction angle, ϕ	35	Degree
Dilation angle, ψ	5	Degree
Shear modulus, G	300	MPa
Bulk modulus, K	971.4	MPa
Gas constant, R	1.987	cal/(molK)
Activation energy, Q	12000	cal/mol
WIPP model exponent, n	4.9	
WIPP model constant, A	4.56	
WIPP model constant, B	127	
WIPP model constant, D	1.4544×10^{-6}	$\text{MPa}^{-\text{n}}\text{s}^{-1}$
Critical steady-state creep rate, $\dot{\epsilon}^*_{ss}$	5.39×10^{-8}	s^{-1}
Temperature, T	300	K

It is shown that the current model can be conveniently used in the context of finite element analysis, and the results of numerical examples are in precise agreement with the available closed-form and finite difference (FLAC) solutions.

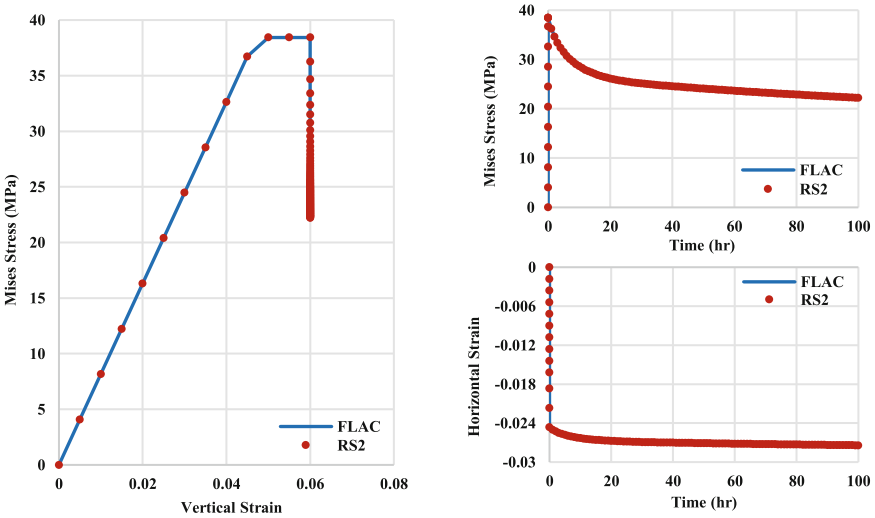

Fig. 13. Finite element (RS2) results compared with finite difference (FLAC) results for the conventional triaxial tests

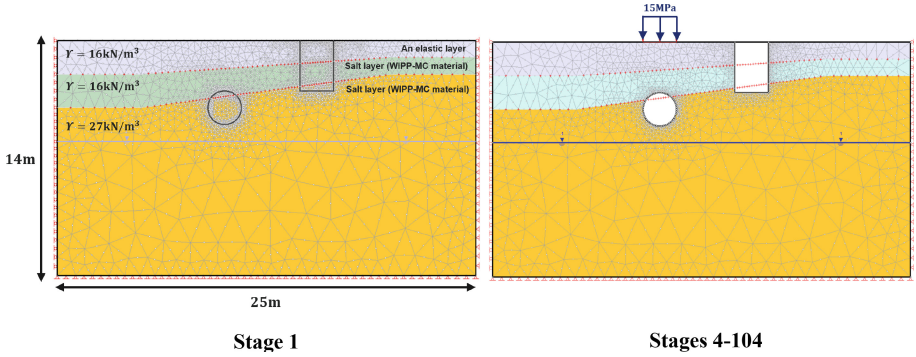

Fig. 14. Configuration and the utilized mesh of the excavation test at different stages

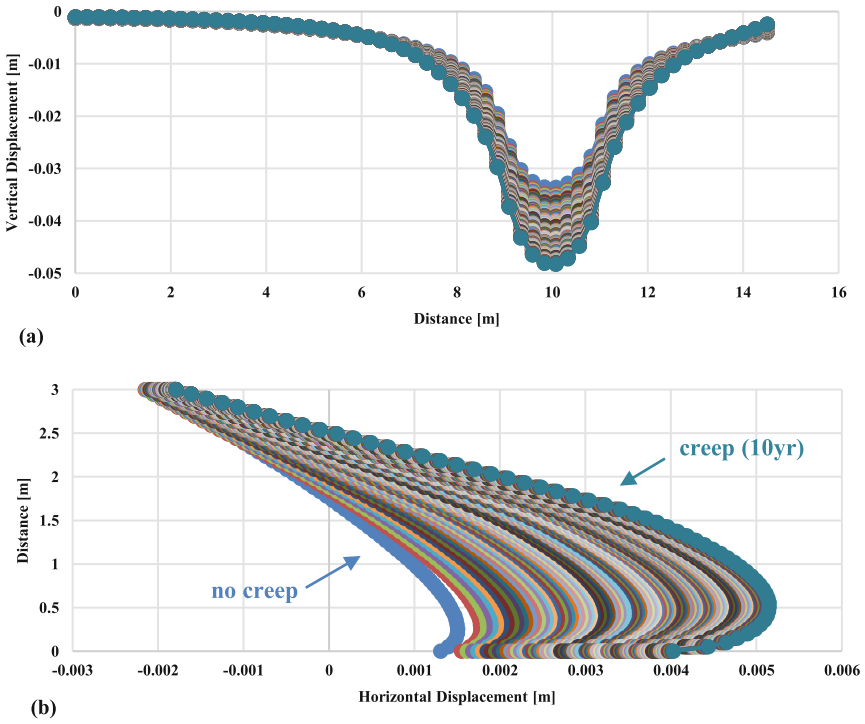

Fig. 15. (a) Settlement of the ground surface above the tunnel, and (b) lateral displacement of the trench wall close to the tunnel

References

Herrmann, W., Wawersik, W. R., Lauson, H.S. *Analysis of Steady State Creep of Southeastern New Mexico Bedded Salt.* Sandia National Laboratories, SAND80-0558 (1980a).

Herrmann, W., Wawersik, W. R., Lauson, H.S. *Creep Curves and Fitting Parameters for Southeastern New Mexico Rock Salt.* Sandia National Laboratories, SAND80-0087 (1980b).

Itasca Consulting Group, Inc. (2019) *FLAC — Fast Lagrangian Analysis of Continua.* Ver. 8.1. Minneapolis: Itasca.

Itasca Consulting Group, Inc. (2019) *UDEC — Universal Distinct Element Code.* Ver. 7.0. Minneapolis: Itasca.

Khan, A. S., Huang, S. *Continuum theory of plasticity.* John Wiley & Sons (1995).

Nayak, G. C., Zienkiewicz, O. C. Convenient form of stress invariants for plasticity. Journal of the Structural Division, 98(4), 949–954 (1972).

Owen, D. R. J., Hinton, E. *Finite elements in plasticity: theory and practice.* Pineridge Press Limited., 285 (1980).

Pietruszczak, S. *Fundamentals of plasticity in geomechanics.* Boca Raton, FL: Crc Press (2010).

Rocscience Inc. 2023. *RS2 – 2D Finite Element Analysis.* www.rocscience.com, Toronto, Ontario, Canada.

Simo, J. C., Hughes, T. J. *Computational Inelasticity.* Springer: New York (1998).

Simo, J. C., Hughes, T. J. R. *Elastoplasticity and Viscoplasticity: Computational Aspects.* Stanford Univ., Division of Applied Mechanics. (1988).

Sjaardema, G. D., Krieg. R. D. *A Constitutive Model for the Consolidation of WIPP (Waste Isolation Pilot Plant) Crushed Salt and Its Use in Analyses of Backfilled Shaft and Drift Configurations*. Sandia National Laboratories, SAND87–1977 (1987).

van Sambeek, L. L. *Creep of Rock Salt under Inhomogeneous Stress Conditions*. Ph.D. Thesis: Colorado School of Mines (1986).